

Privacy Preserved Blood Glucose Level Cross-Prediction: An Asynchronous Decentralized Federated Learning Approach

Chengzhe Piao^a, Taiyu Zhu^b, Yu Wang^a, Stephanie E Baldeweg^{c,d}, Paul Taylor^a, Pantelis Georgiou^e, Jiahao Sun^f, Jun Wang^g and Kezhi Li^{a,*}

^aInstitute of Health Informatics, University College London, London, NW1 2DA, UK

^bDepartment of Psychiatry, University of Oxford, Oxford, OX3 7JX, UK

^cDepartment of Diabetes & Endocrinology, University College London Hospitals, London, NW1 2PG, UK

^dCentre for Obesity & Metabolism, Dept of Experimental & Translational Medicine, University College London, London, WC1E 6JF, UK

^eCentre for Bio-Inspired Technology, Department of Electrical and Electronic Engineering, Imperial College London, London, SW7 2AZ, UK

^fFLock.io, London, WC2H 9JQ, UK

^gDepartment of Computer Science, University College London, London, WC1E 6EA, UK

ARTICLE INFO

Keywords:

Federated Learning
Blood Glucose Prediction
Type 1 Diabetes
Cross-Patient Analysis

ABSTRACT

Newly diagnosed Type 1 Diabetes (T1D) patients often struggle to obtain effective Blood Glucose (BG) prediction models due to the lack of sufficient BG data from Continuous Glucose Monitoring (CGM), presenting a significant “cold start” problem in patient care. Utilizing population models to address this challenge is a potential solution, but collecting patient data for training population models in a privacy-conscious manner is challenging, especially given that such data is often stored on personal devices. Considering the privacy protection and addressing the “cold start” problem in diabetes care, we propose “GluADFL”, blood Glucose prediction by Asynchronous Decentralized Federated Learning. We compared GluADFL with eight baseline methods using four distinct T1D datasets, comprising 298 participants, which demonstrated its superior performance in accurately predicting BG levels for cross-patient analysis. Furthermore, patients’ data might be stored and shared across various communication networks in GluADFL, ranging from highly interconnected (e.g., random, performs the best among others) to more structured topologies (e.g., cluster and ring), suitable for various social networks. The asynchronous training framework supports flexible participation. By adjusting the ratios of inactive participants, we found it remains stable if less than 70% are inactive. Our results confirm that GluADFL offers a practical, privacy-preserving solution for BG prediction in T1D, significantly enhancing the quality of diabetes management.

1. Introduction

Blood Glucose (BG) prediction [1, 2, 3] is indispensable for individuals with Type 1 Diabetes (T1D), as it enables proactive management of BG levels [4, 5], thus preventing potential hyperglycemia and hypoglycemia and mitigating complications. A common challenge faced by many, especially those newly diagnosed or recently initiated on Continuous Glucose Monitoring (CGM) devices, is the lack of sufficient BG trajectory data, leading to a “cold start” issue in developing accurate prediction models. This problem is particularly acute for critically ill patients in intensive care, where timely and effective BG management is crucial [6]. Given that population models can address the cold start problem [7], the emergence of Federated Learning (FL) might offer a promising solution to this challenge, especially in gathering population features while regarding data privacy [8, 9].

Specifically, employing the integration of data from multiple individuals into population models, FL enables the

utilization of patient data on mobile devices or databases in hospitals in a privacy-preserving manner. By directly leveraging the data in the place where it is generated, FL allows for the development of robust prediction models without compromising patient privacy. However, applying FL in the cold start problem triggers some concerns:

- **Target Differences:** In a setting similar to zero-shot learning [10], patients can be categorized as *seen* or *unseen* based on whether their data has been used to train the model. Patients who have been previously observed (*seen* patients) contribute their data to FL training with the expectation of obtaining personalized models. These personalized models are designed to retain the unique behavioral patterns of individual patients. Conversely, patients who have not been previously observed (*unseen* patients) seek a population model by leveraging seen patients’ data. The population model provides them with a foundational starting point, and it is defined as models that encapsulate the general patterns observed across a broad patient cohort (refer to Figure 1).
- **Overhead and Latency:** Learning population models in FL necessitates collecting extensive data from patients. However, scalability and efficiency challenges in managing large-scale data, especially in centralized

*Corresponding author

✉ chengzhe.piao.21@ucl.ac.uk (C. Piao); taiyu.zhu@psych.ox.ac.uk

(T. Zhu); yu.w.23@ucl.ac.uk (Y. Wang); s.baldeweg@ucl.ac.uk (S.E.

Baldeweg); p.taylor@ucl.ac.uk (P. Taylor); pantelis@imperial.ac.uk (P.

Georgiou); sun@flock.io (J. Sun); junwang@cs.ucl.ac.uk (J. Wang);

ken.li@ucl.ac.uk (K. Li)

ORCID(s): 0000-0003-0494-5098 (C. Piao)

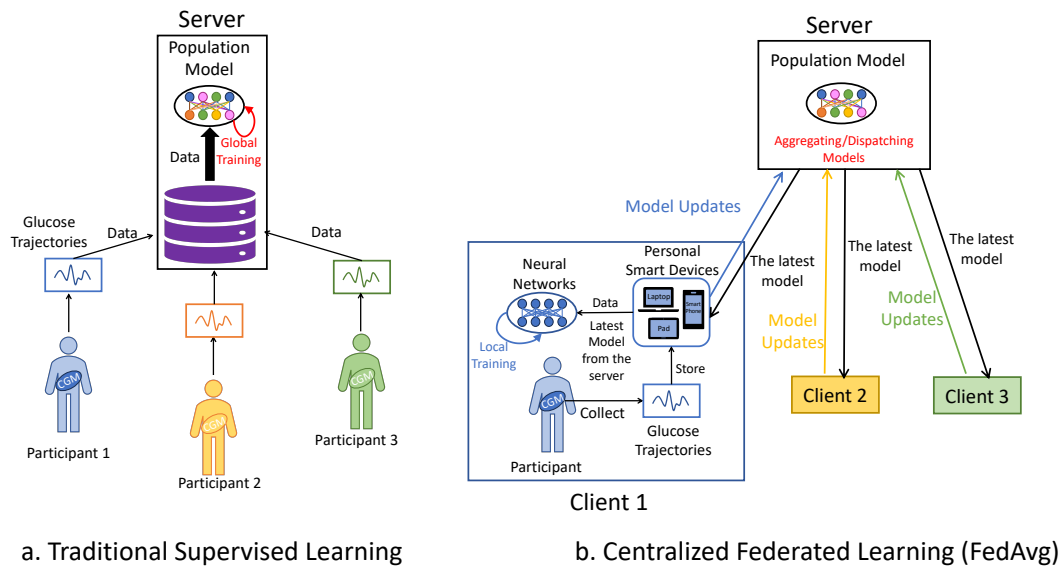


Figure 1: Population models for glucose prediction: a) Traditional Supervised Learning, which centralizes patients’ data on a server to create models by combining data, and b) Centralized Federated Learning (FedAvg, [9]), which utilizes data on personal devices. With FedAvg, only model updates, not raw data, are sent to the server, which then aggregates these updates to improve the population model. This approach maintains data privacy by keeping patient data localized while still benefiting from collective insights. Nevertheless, it has scalability and efficiency challenges in managing large-scale data.

FL (see Figure 1b), are notable due to increasing overhead and latency with more participant devices. These issues are crucial to resolve for practical healthcare applications.

- **Device Limitations:** Patients with basic smartphones might face longer training times due to limited computational resources. Additionally, frequent phone usage can hinder continuous participation in synchronous FL training, reducing overall efficiency.
- **Social Preferences:** Some patients may willingly engage in FL training and allow their devices to communicate broadly, while others may prefer limiting interactions to their social circles.

In order to address the cold start towards unseen patients, the primary objective of FL is to develop a population model that leverages data from seen patients while safeguarding their privacy (Figure 1). This population model is intended to be applicable to both *seen* and *unseen* patients, which sets it apart from most existing work that focuses on personalized BG prediction. However, in this study, we also introduce a “personalized from population” approach that further fine-tunes the population model to better suit each patient’s unique characteristics. Specifically, seen patients can leverage their mobile devices such as smart phones to engage in FL training. Such devices are equipped with storage for CGM sensor data, and tools like TensorFlow Lite support on-device training¹. After developing the population model, seen patients can further optionally personalize the model with their data, i.e., “personalized from population”.

¹https://www.tensorflow.org/lite/examples/on_device_training/overview

Meanwhile, unseen patients can initially use the population model with a “warm” start. They can even subsequently fine-tune it as they collect more personal data. Throughout this process, the privacy of personal data is safeguarded, as it remains confined to the individual’s device.

Then, given other concerns, a centralized FL structure fails to offer viable solutions. Therefore, we propose “GluADFL”, a Glucose management system using Asynchronous Decentralized FL. Removing the central server allows our method to be scalable for large-scale data applications. This system accommodates various communication topologies (ring, cluster, random), catering to diverse social needs. By enabling asynchronous training, it mitigates the impact of “slow” and “busy” devices, allowing broader and more convenient participation in the training process. Meanwhile, as demonstrated in the BG level prediction challenge 2020 [11], Long Short-Term Memory (LSTM) models [12, 13] have proven their efficacy. Besides, well-developed APIs for LSTM models, such as TensorFlow or PyTorch, are widely supported across a broad range of mobile devices. Conversely, other models, such as Neural Basis Expansion Analysis for interpretable Time Series (N-BEATS, [14]), Neural Hierarchical interpolation for Time Series (NHITS, [15]) or customized transformers [16], have yet to receive similar support. Therefore, we choose LSTM as the prediction method for GluADFL due to its reliable performance and well developed APIs on mobile devices.

To evaluate GluADFL with LSTM, our experiments consider four diverse datasets, involving 298 participants. Our findings are summarized as follows:

- The LSTM-based population model, trained through GluADFL, possesses the capability to cross-predict,

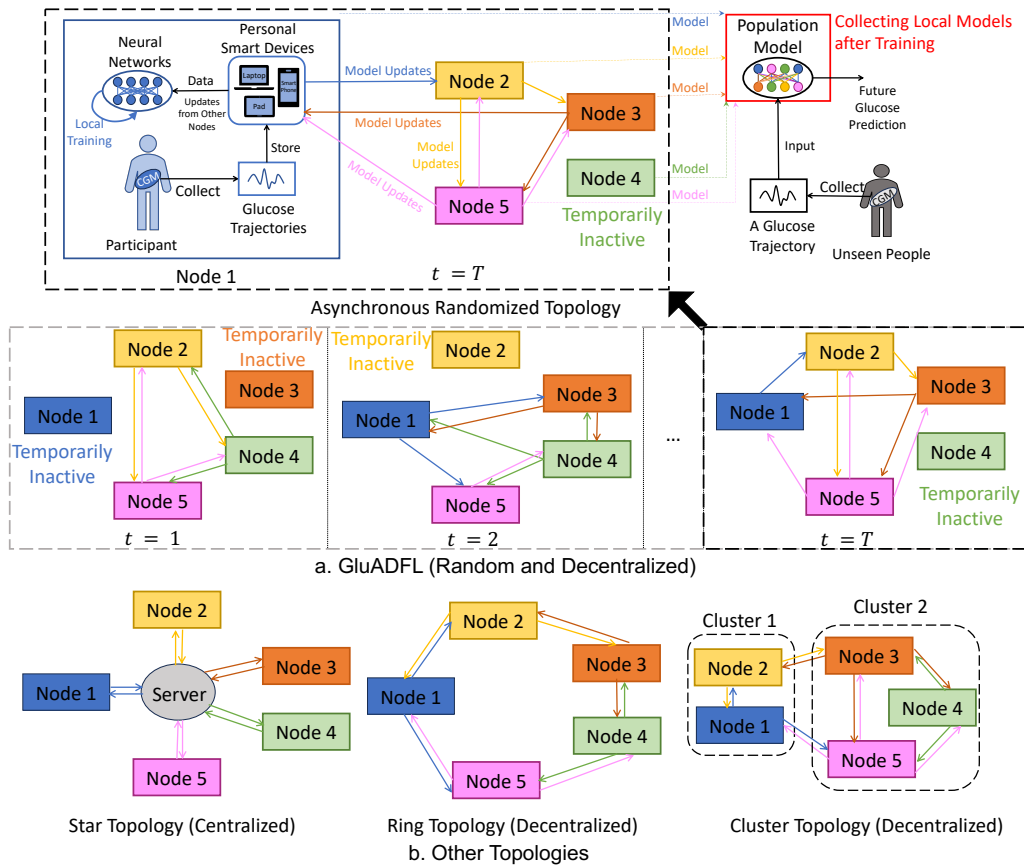


Figure 2: A Glucose management system using Asynchronous Decentralized Federated Learning (GluADFL), tailored for Type 1 Diabetes (T1D) management. Figure a showcases the GluADFL employing randomized communication graphs, highlighting the dynamic nature of node interactions for distributed learning. Nodes can mirror the participants (seen patients) attending the training. In these nodes, through CGM devices, glucose data is collected and processed on local devices for model training. Engaging in the GluADFL process, these devices collaboratively develop a population model to enhance BG management for both seen patients with ample CGM data and unseen patients lacking sufficient data. Figure b presents other three distinct communication graph topologies: star, ring, and cluster. Star topology is only for centralized FL (FedAvg [9]). Random, ring and cluster can be utilized in GluADFL, each catering to different operational efficiencies and privacy considerations within the network. These topologies reflect diverse participant preferences for data sharing and communication.

meaning it can accurately predict BG levels for unseen patients. Additionally, fine-tuning this model with data from seen patients results in personalized models that significantly outperform those created from random initialization. Along with the safe privacy, this improvement in BG prediction is an attractive incentive for seen patients to participate in FL training to refine their personalized models.

- We evaluate the performance of GluADFL across different communication topologies, i.e., ring, cluster, and random, to cater to various social needs. The random topology emerges as relatively the most effective, showing a tendency to converge with the best performance. To assess the robustness of GluADFL in asynchronous environments, we experiment with varying inactive node ratios. This approach simulates the impact of different levels of participant inactivity on the training efficiency of the population model. We observe that in a random-based GluADFL setting,

the training framework’s effectiveness is significantly impacted only when the proportion of inactive nodes exceeds 70%.

- We compare the cross-patient BG prediction capabilities of GluADFL with eight distinct methods. When training population models using seen patients’ data via traditional supervised learning, the LSTM-based approach outperforms other methods such as linear regression, eXtreme Gradient Boosting (XGBoost [17]), N-BEATS, [14], and NHITS [15], validating LSTM as a practical choice for population modeling. Furthermore, the GluADFL-based models achieve comparable performance to supervised learning and centralized FL [9], and they are superior to the meta-learning framework [18, 19] without fine-tuning. This highlights the robust cross-predictive capability of GluADFL-based LSTM population models.

2. Related Work

FL has significantly evolved since its initial concept with FedAvg [9], a centralized model involving a server coordinating multiple clients. FedAvg’s core principle is to train models directly on devices where data originates, avoiding the need for centralized data gathering and enhancing privacy protection.

Decentralized FL has further evolved from this concept by eliminating the central server, enabling broader participation. Various researchers have proposed innovative decentralized FL frameworks. For instance, He *et al.* [20] introduced SpreadGNN, a multi-task federated framework adept at handling partial labels without a central server. Shi *et al.* [21] developed DFedSAM and DFedSAM-MGS, the former utilizing gradient perturbation for local model flattening, and the latter enhancing this with Multiple Gossip Steps for improved model consistency and communication balance. Liu *et al.* [22] implemented a method balancing communication efficiency and model consensus through periodic local updates and inter-node communications. Chen *et al.* [23] optimized resource efficiency by limiting gradient pushes to a neighbor subset. Dai *et al.* [24] and Bornstein *et al.* [25] explored various decentralized communication topologies, such as random, ring, and cluster, offering potential solutions for diverse social needs.

Asynchronous FL represents a significant advancement in FL methodologies. This variation has been explored in various studies. Hagos *et al.* [26] ventured beyond centralized FL by investigating scalable asynchronous FL techniques for privacy-preserving real-time surveillance systems, demonstrating its practical applications. Jang *et al.* [27] introduced AsyncFL, a system where clients upload models based on their capabilities, and the FL server asynchronously updates and broadcasts the global model, showcasing the flexibility of asynchronous operations. Yang *et al.* [28] developed Anarchic FL, allowing workers to decide their participation schedule and the extent of local computations in each round, emphasizing the autonomy in centralized FL settings. Bornstein *et al.* [25] proposed SWIFT for decentralized FL, enabling participants to join training asynchronously and broadcast model parameters at their convenience, highlighting the adaptability in decentralized environments.

FL plays a pivotal role in ensuring data security and privacy, adhering to strict regulations like the EU/UK General Data Protection Regulation, thereby becoming increasingly relevant in healthcare [29]. Its application across various healthcare scenarios [30, 31, 32, 33], especially including diabetes detection [34] and prediction [35, 36], and glucose prediction [37], underscores its significance in protecting healthcare data. Notably, Falco *et al.* [37] introduced a FL framework using an evolutionary algorithm in diabetes management marks a significant stride in privacy-focused glucose prediction. However, existing studies in healthcare often overlook the full potential of FL in terms of generalization, scalability, and asynchronous updates, essential for real-world healthcare implementation. Centralized

training frameworks fall short in addressing diverse “social preferences” and “device limitations”. To the best of our knowledge, our proposed approach, GluADFL, is the first work that overcomes these limitations by employing asynchronous decentralized FL aided by various communication graphs for learning population models, thus enhancing the practicality and applicability of FL in healthcare.

3. Proposed Method

3.1. Problem Definition

Our goal is to develop an asynchronous decentralized FL framework, aimed at enhancing diabetes management for both seen and unseen patients. While this support initially focuses on Blood Glucose Level Prediction (BGLP), it’s designed to be adaptable for broader applications such as insulin guidance, dietary recommendations, and other critical aspects of life-cycle management. In this paper, we concentrate specifically on BGLP.

BGLP (BG only): We define BGLP as the task of predicting future glucose levels x_{L+H} , based on a series of historical glucose records $x_{1:L} = \{x_1, \dots, x_L\}$, collected through CGM at regular intervals δl (e.g., every 5 minutes). The prediction horizon, denoted as H , is the future time when the prediction is made (e.g., $H = 6$ equals to 30 minutes ahead).

Our approach focuses on using univariate glucose series, denoted as $x_{1:L}$. This approach stems from the practical challenges in collecting high-quality data via a full suite of wearable devices from all patients [38] and ensuring their comfort with wearing multiple sensors. Self-reported data also presents the risk of artifacts and errors in logging [39] and could lead to an unpleasant user experience due to the frequent need for manual entry. Thus, relying solely on CGM data emerges as a more convenient and accurate method for future BG predictions. This decision aligns with research underscoring the substantial impact of glucose trajectories on prediction accuracy [40, 41, 42]. For instance, our previous work [40] has demonstrated that CGM data and timestamps together contribute significantly (93.9%) to future BG level predictions, with the major contribution attributed to CGM. Meanwhile, there is substantial variability in self-reported events among individuals, which can impair the predictive performance of population models. This issue is particularly crucial for FL that aims to generalize models across diverse populations.

An additional benefit of adopting a univariate approach is the optimization of computational resources and its effective performance, especially in LSTM models [12, 43]. This not only enhances performance but also significantly reduces the training load on mobile devices, making the process more efficient and feasible for widespread use in patient care.

3.2. Problem Formulation

As outlined in section 1, our objective is to utilize FL for developing a population model that addresses the “cold

start” issue for unseen patients while simultaneously enhancing the prediction accuracy of personalized models for seen patients. The population model is characterized as follows:

Population Modeling: Given a set of patients $\mathcal{N} = \{1, \dots, n, \dots, N\}$, where each patient n possesses a private dataset \mathcal{X}^n , our goal is to derive a population model $\hat{x}_{L+H}^n = f(x_{1:L}^n; \mathbf{w})$ for all n in \mathcal{N} , with \mathbf{w} representing the model’s learnable parameters, and H is the prediction horizon.

In contrast to the personalized model $f(x_{1:L}^n; \mathbf{w}^n)$, which tailors to individual data of the patient n , the population model $f(x_{1:L}^n; \mathbf{w})$ utilizes non-personalized parameters \mathbf{w} to capture universal patient patterns [12]. This approach effectively tackles the “cold start” issue for patients not previously encountered in the model [7]. In this work, we adopt the LSTM [44] for the population model. The LSTM framework captures long-term dependencies via its self-gated mechanism, which includes input, forget, and output gates, allowing for effective information flow management. Unlike convolutional methods that lack memory for long-term sequences, LSTM excels in recognizing patterns over extended periods. Moreover, this technology strikes an optimal balance by offering the capacity to learn complex temporal patterns with minimal need for extensive hyperparameter tuning, ensuring both resource conservation and effective performance in constrained environments. Its blend of computational efficiency, effectiveness, and the presence of well-developed APIs renders it particularly suitable for mobile devices.

Furthermore, we aim to adopt decentralized FL to facilitate increased participation without the scalability constraints associated with a central server. This approach encourages a broader inclusion of participant data in the learning process.

Decentralized FL: In a decentralized FL setup, nodes $\mathcal{N} = \{1, \dots, n, \dots, N\}$ are interconnected via a communication graph \mathcal{G} , mirroring the patient set \mathcal{N} . Each patient n corresponds to a node in \mathcal{G} , with the graph’s edges representing the communication links between patients. As for node n , this topology allows it to direct communicate with its neighboring nodes \mathcal{N}^n connected by one-hop links. The decentralized FL framework aims to optimize a global function:

$$\min_{\mathbf{w}} \sum_n J(x_{L+H}^n, \mathbf{w}), \quad (1)$$

where the loss function for the BGLP at each node n is defined as:

$$J(x_{L+H}^n, \mathbf{w}) = \mathbb{E}_{x^n \sim \mathcal{X}^n} [(x_{L+H}^n - f(x_{1:L}^n; \mathbf{w}))^2], \quad (2)$$

aiming to minimize the mean square error of all nodes between predicted and actual BG levels, thus improving prediction accuracy in BGLP through collaborative learning without centralized control.

3.3. Proposed Asynchronous Decentralized FL for Learning a Population Model in BGLP

Figure 2a depicts participants (seen patients with T1D who possess sufficient CGM data) as nodes in the communication graph \mathcal{G} , representing a network that can adopt ring, cluster, or random topologies as shown in Figure 2b. This topology choice is based on the participants’ communication preferences. CGM devices collect glucose data for processing and training on local devices. These devices engage in GluADFL, an asynchronous decentralized FL process for BGLP, working collectively to create a population model that supports BG management for new users (unseen patients with T1D who do not have enough CGM data).

The GluADFL process entails:

- **Step 1 - Initial Setup:** Node models are initialized with random parameters (Line 3).
- **Step 2 - Broadcasting:** Active nodes share their model parameters with nearby active nodes, influenced by \mathcal{G} ’s topology (Line 5).
- **Step 3 - Local Model Aggregation:** Each active node update its model by averaging its own model and the received models from neighbors (Lines 7-9).
- **Step 4 - Local Training:** Nodes refine their models using their data based on aggregated parameters (Lines 11-13).
- **Step 5 - Iterative Learning:** Steps 2-4 are repeated asynchronously until achieving convergence or meeting a stop condition.
- **Step 6 - Population Model Formation:** Final model parameters are aggregated from all nodes to form the population model (Lines 15-16).

Convergence (in step 5) within the context of GluADFL can be defined as reaching a state where the objective function, as detailed in Equation (2), cannot be minimized any further. This indicates that the model has reached its optimal performance, and further iterations do not yield significant improvements in prediction accuracy. Additional stopping criteria for the algorithm can include specific thresholds for the objective function. This allows for flexibility in determining when the learning process has reached a satisfactory level of performance or optimization, providing a practical mechanism for stopping the algorithm under predefined conditions.

The algorithm enables the direct application of the population model for unseen patients, offering immediate benefits in BG management. Seen patients, who have contributed their data, have the flexibility to further refine this population model with their own data, utilizing Equation (2) and adjusting the learning rate γ for personalization. This customization process enhances the model’s relevance to the individual’s unique data patterns. Moreover, seen patients might also directly use the population model, as it often

Algorithm 1: GluADFL

```

1 Input: Training steps  $T$ , set of nodes  $\mathcal{N}$ , max
   communication batch size  $B$ , initial model
   parameters  $\{\mathbf{w}_0^n\}_1^N$ , learning rate  $\gamma$ , and training
   data  $\{\mathcal{X}^n\}_1^N$ 
2 Output: Population model  $\mathbf{w}$ 
3 Initialize node models in  $\mathcal{N}$  with  $\{\mathbf{w}_0^n\}_1^N$ 
4 for  $t = 1$  to  $T$  do
5     Broadcast model parameters from active nodes
      to their neighbors, depending on the current
      communication graph
6     # Model updates post-broadcast
7     for  $n = 1$  to  $N$  do
8         if node  $n$  is active then
9             Update node  $n$ 's model with the
              neighbor node set  $\mathcal{N}_t^n$ , ensuring
               $|\mathcal{N}_t^n| \leq B$ :  $\hat{\mathbf{w}}_{t-1}^n \leftarrow$ 
               $\frac{1}{|\mathcal{N}_t^n|+1} \left( \sum_{n' \in \mathcal{N}_t^n} \mathbf{w}_{t-1}^{n'} + \mathbf{w}_{t-1}^n \right)$ 
10        # Node model updates with local data
11        for  $n = 1$  to  $N$  do
12            if node  $n$  is active then
13                Update using local data:
                   $\mathbf{w}_t^n \leftarrow \hat{\mathbf{w}}_{t-1}^n - \gamma \nabla J(x_{L+H}^n, \mathbf{w}_{t-1}^n)$ 
14 # Finalize the population model  $\mathbf{w}$ 
15 Aggregate model parameters from all nodes
16  $\mathbf{w} \leftarrow \frac{1}{N} \sum_n \mathbf{w}_T^n$ 

```

surpasses solely personalized models that lack population-derived insights, providing a robust starting point for individual adaptations.

The GluADFL framework facilitates asynchronous communication [25], allowing nodes to update their models or pause without waiting for others, enhancing flexibility and efficiency. Nodes can rejoin the learning process when ready, ensuring that each participant contributes at their own pace. This wait-free mechanism supports continuous local model improvements and collective learning without the need for synchronous updates, making the learning process more adaptable to individual and network variabilities.

In the GluADFL framework, we explore three distinct communication graphs to facilitate model training and parameter sharing:

- **Random** [24]: As illustrated in Figure 2a, active nodes randomly establish connections with up to B other active nodes for exchanging model parameters. This topology introduces a flexible and dynamically changing network structure at each training step.
- **Cluster** [25]: Initially, nodes are organized into clusters, creating a ring-like structure where each cluster is

fully connected internally and linked to others through specific nodes. This setup, shown in Figure 2b, promotes efficient intra- and inter-cluster communication, with the structure remaining constant throughout training.

- **Ring** [25]: Nodes are arranged in a circular pattern, enabling sequential parameter sharing along the ring. This ensures a consistent, cyclic flow of information among all active participants, depicted in Figure 2b, with the communication pattern fixed during the training.

The choice of communication graphs in GluADFL can cater to diverse social preferences and privacy concerns of participants. The random topology fits scenarios where participants are open to broader interaction beyond their immediate social circles. The cluster topology is ideal for those preferring interactions within known groups, resembling social circles. For utmost privacy, the ring topology allows communication exclusively between two closely connected individuals, mirroring the preference to limit data (model parameters) sharing to a minimum. Thus, these topologies offer customizable communication settings to meet varied social and privacy needs.

These communication graphs enhance the distributed nature of communication and decrease dependency on a single master node, characteristic of the star topology in FedAvg [9], as illustrated in Figure 2b. By facilitating efficient, decentralized exchanges among participants, these structures foster collaboration and accelerate the learning process for BGLP, offering a more resilient and scalable approach to FL.

4. Experiments and Results

4.1. Datasets

All the results are based on the prediction of future BG levels for patients with T1D using OhioT1DM [11], ABC4D ([45, 3], NCT02053051), CTR3 (NCT02137512) and REPLACE-BG ([46], NCT02258373). The statistics for these four datasets are presented in Table 1, highlighting their diversity. For example, the ABC4D dataset delivered insulin exclusively using pens (Novo Nordisk Echo), whereas other datasets leveraged pumps. This potentially makes the BG variability the greatest in ABC4D, resulting in a challenging BG prediction. Each dataset, excluding OhioT1DM, is divided into training (60%), validation (20%) and testing data (20%) by time per person. As for OhioT1DM, it has been originally divided into training and testing data. We make the last 20% of its training data as the validation data. As mentioned in section 3.1, only BG time series is considered. Hence, we leveraged Z-Score normalization to standardize the BG levels within each dataset using the mean and standard deviation of training data, then all missing values are replaced with zero [12].

Table 1

The statistics of four datasets

Demographic	OhioT1DM	ABC4D	CTR3	REPLACE-BG
CGM	Medtronic Enlite	Dexcom G5	Dexcom G4	Dexcom G4
Insulin Pump or Pen	MiniMed 530G/630G	Novo Nordisk Echo	Roche Accu-Chek	MiniMed 530G, OmniPod, etc.
No. of Participants	12	25	30	226
No. of Days	54(2)	168(14)	163(67)	251(39)
No. of CGM Records per Participant	13871(1015)	43259(5460)	43421(18309)	66153(10701)
Mean of CGM Data (mg/dL)	159.35(16.34)	156.66(24.24)	151.37(13.34)	160.69(21.18)
SD of CGM Data (mg/dL)	58.11(6.15)	60.52(14.47)	55.29(8.24)	60.33(11.65)
Time In Range (%)	63.54(9.70)	62.54(15.58)	69.92(7.95)	63.10(12.18)
Time Below Range (%)	3.30(2.25)	6.01(4.13)	3.53(2.11)	3.78(2.51)
Time Above Range (%)	33.15(10.71)	31.45(15.65)	26.54(8.57)	33.13(12.93)
Coefficient of Variation (%)	36.63(3.70)	38.40(6.22)	36.44(3.90)	37.45(4.70)
Low Blood Glucose Index	0.88(0.48)	1.73(1.02)	0.97(0.48)	1.00(0.58)
High Blood Glucose Index	7.15(2.45)	7.26(3.85)	5.89(1.93)	7.57(3.42)

4.2. Ethics and Data availability

All datasets can be accessed publicly apart from ABC4D, which can be accessed via authorised procedures by contacting the project manager and the corresponding author. The ABC4D studies were conducted under protocol (13/LO/0264) approved by the London - Chelsea Research Ethics Committee in 2013.

4.3. Metrics

In this study, the metrics used to evaluate the performance of the BGLP includes root mean square error (RMSE), mean absolute relative difference (MARD), mean absolute error (MAE), glucose-specific RMSE (gRMSE, [47, 48]) and time lag. RMSE (mg/dL) measures the square root of the average of the squares of the errors, as follows (I is the total number of testing examples):

$$RMSE = \sqrt{\frac{1}{I} \sum_i (x_{L+H,i} - \hat{x}_{L+H,i})^2}. \quad (3)$$

MARD (%) averages the absolute differences between predicted and actual values, expressed as a percentage of the actual values. It is used to assess the relative accuracy of the predictions.

$$MARD = \frac{1}{I} \sum_i \frac{|x_{L+H,i} - \hat{x}_{L+H,i}|}{x_{L+H,i}} \times 100\%. \quad (4)$$

MAE (mg/dL) measures the average of the absolute differences between the predicted values and the actual values. Without squaring the errors before averaging allows it to be less sensitive to large errors than RMSE.

$$MAE = \frac{1}{I} \sum_i |x_{L+H,i} - \hat{x}_{L+H,i}|. \quad (5)$$

gRMSE (mg/dL) is a variation of RMSE, evaluating the prediction error specifically within certain ranges of BG levels. It allows for a more detailed assessment of model performance across different glucose level ranges, which is crucial in diabetes management where different ranges

(e.g., hypoglycemia, hyperglycemia) have different clinical implications.

$$gRMSE = \sqrt{\frac{1}{I} \sum_i P(x_{L+H,i}, \hat{x}_{L+H,i})(x_{L+H,i} - \hat{x}_{L+H,i})^2}, \quad (6)$$

where $P(x_{L+H,i}, \hat{x}_{L+H,i})$ penalizes overestimation in hypoglycemia and underestimation in hyperglycemia, and more details are in [47].

In BGLP, time lag (minutes) quantifies the temporal discrepancy between actual BG level changes and when these changes are detected by the model's predictions. This concept, as detailed by Cohen [49] through cross-correlation analysis, and further applied in BGLP contexts [50, 51], highlights the critical challenge of timely and accurate BG prediction, emphasizing the importance of minimizing lag for effective diabetes management.

In summary, we pursue lower values of all these metrics, meaning better prediction models for BGLP.

4.4. Baselines

In our experiments, several baselines were compared with the proposed model. First of all, five kinds of population models were gotten by traditional supervised learning through mixing the training data of all patients within each dataset as follows:

- **LR**: it is a Linear Regression (LR) model that predicts values based on linear relationships between input features and target variable.
- **XGBoost** [17]: it is based on gradient boosting, leveraging decision trees and optimizing model performance through sequential learning.
- **LSTM**: a single layer of LSTM whose self-gated mechanisms can model long short-term patterns of time series.
- **N-BEATS** [14]: it is a Neural Basis Expansion Analysis for interpretable Time Series (N-BEATS) forecasting through leveraging a stack of fully-connected layers and backcasting.

- **NHiTS** [15]: it is a Neural Hierarchical Interpolation for Time Series (NHiTS), leveraging hierarchical interpolation and pooling techniques. Compared with N-BEATS, it improves time series predictions by specializing in different frequencies and reducing computational complexity.

Furthermore, we introduced meta-learning methods and centralized FL to our baselines for comparisons.

- **MAML** [18]: an LSTM model trained by Model-Agnostic Meta-Learning (MAML). MAML is to find a set of initial parameters that can quickly adapt to new tasks through few gradient updates.
- **MetaSGD** [19]: an LSTM model trained by Meta-learner acting like Stochastic Gradient Descent (MetaSGD). MetaSGD extends MAML by introducing a learnable learning rate for each parameter in the model, providing more flexibility and potentially to various tasks.
- **FedAvg** [9]: an LSTM model trained by using centralized Federated Averaging (FedAvg) method. It has a centralized server to periodically broadcast latest model parameters to local devices and average the local model parameters which are trained separately by local data.

Then, our proposed method with three different communication graphs are denoted as “GluADFL(Ring)”, “GluADFL(Cluster)” and “GluADFL(Random)”.

We set the historical BG series length as $L = 12$, i.e., 2 hours, predicting the BG level in 30 minutes ($H = 6$). Except for LR, each method was trained four times with different random seeds. We leverage grid search for selecting the hyperparameters of XGBoost. We implemented all deep learning methods using PyTorch 1.11.0, based on [52, 53] and PyTorch Forecasting², and executed them on an NVIDIA RTX 3090 Ti. For deep learning methods, the learning rate was found in $\{10^{-3}, 10^{-4}, 10^{-5}\}$ and the hidden state size was found in $\{128, 256, 512\}$. The best hyperparameters were selected based on validation data performance. All experiments and results can be accessible and reproducible: “<https://github.com/ChengzhePiao/coldstartbglp>”.

4.5. Results

To assess the cross-prediction capabilities of population models for unseen patients, we compare the performance of population LSTM models trained via the “GluADFL(Random)” approach (Table 2) and traditional supervised learning (Table 3) across four distinct datasets. Performance is evaluated using testing data from all datasets, with specific interest in the off-diagonal cells (non-bold) in Tables 2 and 3, which represent predictions for unseen patients. In the analysis, differences in performance between seen and unseen patients are categorized by color: differences below 0.30 or between (0.3, 0.5] are marked in red or blue, respectively. In Table 2, 78% of metrics for unseen patients show

Table 2

Generalization of population models trained by GluADFL

Training Data	Metric	Testing Data			
		OhioT1DM	ABC4D	CTR3	REPLACE-BG
OhioT1DM	RMSE	19.66(2.52)	23.61(4.44)	20.49(3.23)	20.73(3.45)
	MARD	9.43(1.62)	12.97(3.73)	10.38(1.50)	10.71(1.95)
	MAE	13.80(1.61)	16.25(2.42)	14.41(2.24)	14.75(2.45)
	gRMSE	24.61(3.35)	30.65(7.00)	25.15(4.27)	25.98(4.67)
	Time Lag	5.22(4.48)	6.54(5.05)	10.31(3.97)	9.41(3.99)
ABC4D	RMSE	19.74(2.56)	22.28(4.03)	20.08(3.21)	20.21(3.22)
	MARD	9.45(1.61)	12.16(3.22)	10.13(1.51)	10.43(1.85)
	MAE	13.88(1.59)	15.41(2.05)	14.11(2.23)	14.43(2.34)
	gRMSE	24.69(3.26)	28.60(6.34)	24.57(4.20)	25.28(4.32)
	Time Lag	5.36(4.17)	6.69(4.90)	10.37(4.01)	9.51(3.87)
CTR3	RMSE	19.76(2.61)	22.79(4.19)	20.00(3.13)	20.28(3.27)
	MARD	9.45(1.62)	12.55(3.54)	10.09(1.47)	10.49(1.87)
	MAE	13.83(1.57)	15.73(2.19)	14.03(2.17)	14.44(2.34)
	gRMSE	24.71(3.42)	29.46(6.66)	24.42(4.07)	25.36(4.41)
	Time Lag	5.01(3.76)	6.35(4.81)	9.76(3.79)	9.02(3.79)
REPLACE-BG	RMSE	19.75(2.61)	22.97(4.26)	20.17(3.20)	20.34(3.32)
	MARD	9.38(1.61)	12.54(3.46)	10.17(1.50)	10.45(1.88)
	MAE	13.80(1.59)	15.77(2.19)	14.14(2.21)	14.44(2.36)
	gRMSE	24.62(3.40)	29.68(6.74)	24.61(4.15)	25.38(4.47)
	Time Lag	5.56(4.46)	6.64(4.95)	10.38(4.10)	9.46(3.93)

Bold: results for seen patients (diagonal);

Un-Bold: results for unseen patients (non-diagonal);

Red: differences between seen patients and unseen patients are below 0.30 for each column;

Blue: differences between seen patients and unseen patients are between (0.3, 0.5] for each column.

minor discrepancies (≤ 0.50) compared to seen patients. Excluding models trained with the OhioT1DM dataset, this percentage rises to 87%, suggesting a high level of predictive consistency across different patient groups. This indicates that models trained through GluADFL generally maintain uniform accuracy. However, models trained specifically with OhioT1DM data display weaker generalization, mainly due to the dataset’s smaller size. Similarly, in Table 3, 80% of metrics for unseen patients are closely matched (≤ 0.50) with those of seen patients, increasing to 88% when excluding OhioT1DM-trained models, showcasing the inherent generalization capability of the population models by traditional supervised learning across patient data. Incorporating FL preserves this capability with only a slight reduction.

In Figure 3, we examine “Personalized Model”, “Population Model”, and “Personalized from Population” across four datasets, focusing on the advantage for seen patients participating in FL training. A “Personalized Model” starts with a randomly initialized model for each participant, individually tailored with their data. The “Population Model” is derived from “GluADFL”. “Personalized from Population” allows further refining the population model with personal data, enhancing it into a personalized model. In terms of RMSE, “Personalized from Population” outperforms “Personalized Model” by 0.83, 0.75, 0.40, and 0.44 mg/dL, and in terms of gRMSE, by 1.07, 1.07, 0.62, and 0.57 mg/dL across the datasets, indicating significant benefits for seen patients from incorporating population features through FL training.

In our analysis, we investigate the impact of different typologies of GluADFL on the training process, as depicted in Figure 4. We observe that, towards the end of the communication rounds, the performance of “GluADFL(Random)” surpasses that of “GluADFL(Ring)” across various datasets. Specifically, improvements in RMSE for “GluADFL(Random)” compared to “GluADFL(Ring)” are noted as 0.06, 0.48, 0.28, and 0.53 mg/dL for OhioT1DM, ABC4D, CTR3, and REPLACE-BG datasets, respectively. The performance of

²<https://github.com/jdb78/pytorch-forecasting>

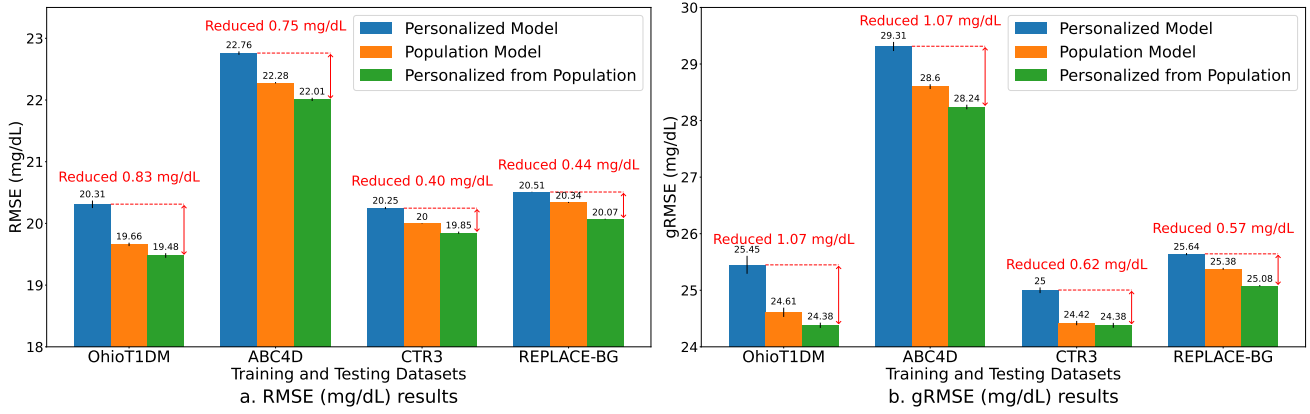


Figure 3: Evaluation of “Personalized Model”, “Population Model”, and “Personalized from Population” across four datasets. The “Personalized Model” involves individual models for each patient, originally randomly initialized and trained with the patient’s own data. The “Population Model” is derived from the GluADFL framework using a random topology and trained by mixing patients’ data. “Personalized from Population” approach refines the GluADFL-based population model by integrating individual patient data to create a customized model, offering a hybrid approach that leverages both broad population insights and specific patient data.

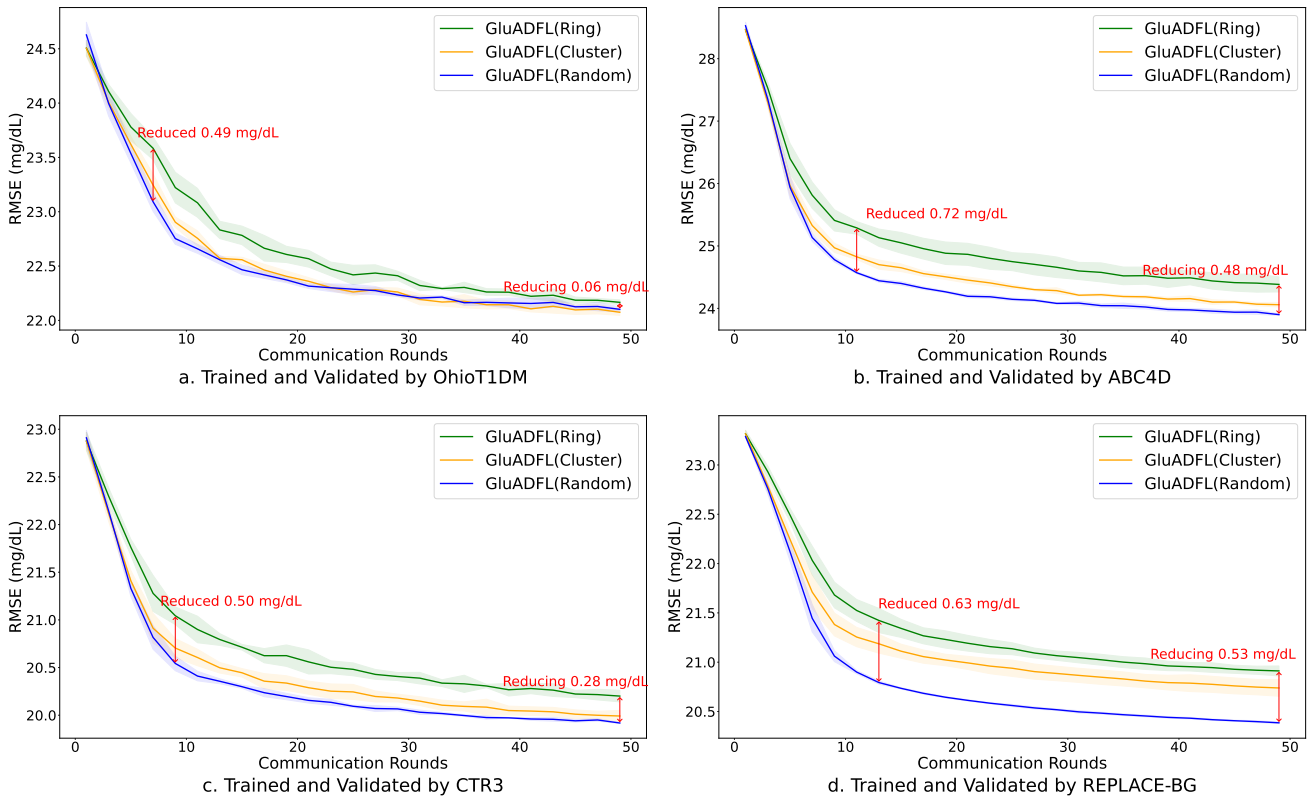


Figure 4: The convergence of population models trained by GluADFL with different communication graphs on four datasets.

“GluADFL(Cluster)” is found to be intermediate between the two.

Furthermore, we assess the influence of varying inactive participant proportions during the training phases on the overall performance across different topologies, as shown in Figure 5. The evaluation highlight that with a 90% inactive node ratio, “GluADFL(Random)” demonstrates a

reduction in RMSE by 1.40, 1.28, and 1.09 mg/dL on the OhioT1DM, ABC4D, and CTR3 datasets, respectively, when compared with “GluADFL(Ring)”. Additionally, at a 70% inactive node ratio, “GluADFL(Random)” shows a reduction in RMSE by 1.19 mg/dL on the REPLACE-BG dataset compared with “GluADFL(Ring)”. Overall, “GluADFL(Random)” achieve an average reduction in RMSE

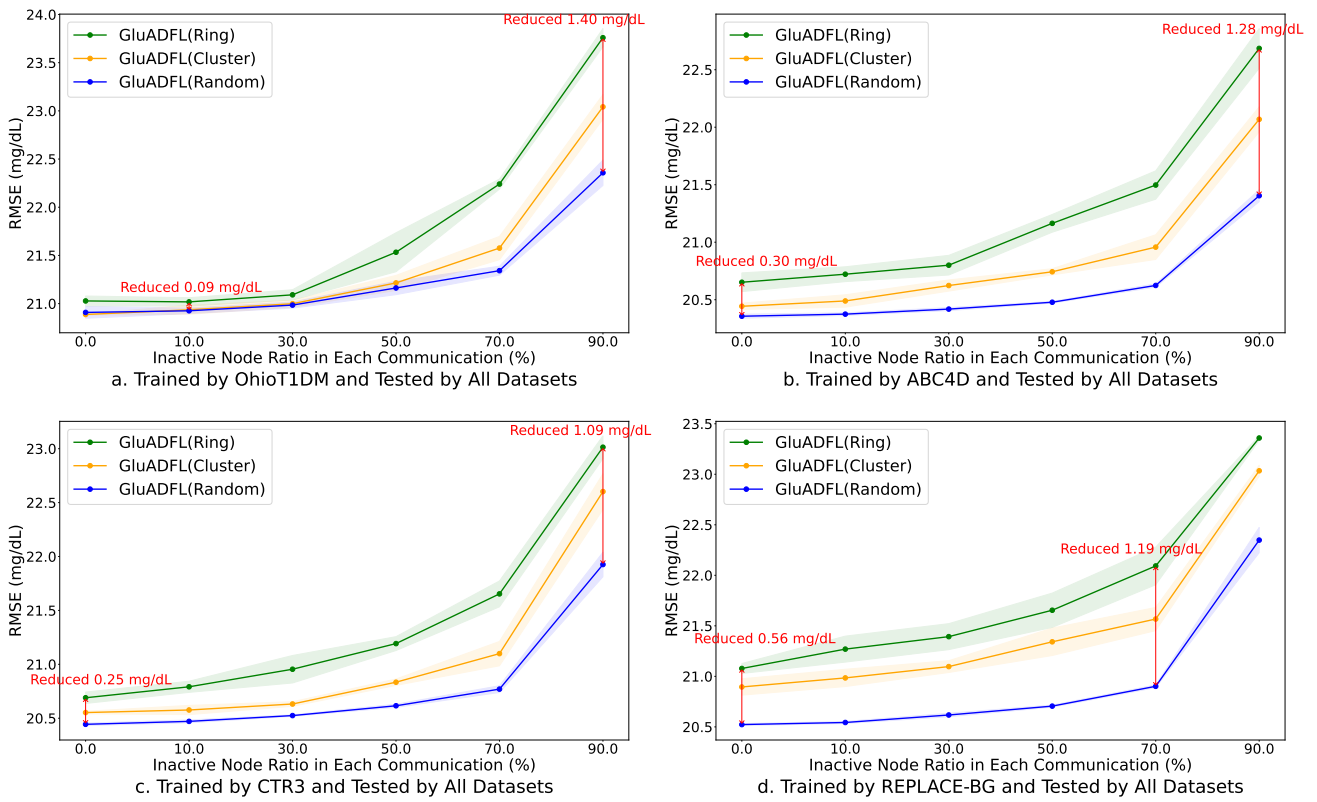


Figure 5: The performance of GluADFL with different communication topology when changing inactive node ratio in each communication.

Table 3
 Generalization of population models trained by mixing data

Training Data	Metric	Testing Data			
		OhioT1DM	ABC4D	CTR3	REPLACE-BG
OhioT1DM	RMSE	19.65(2.48)	23.59(4.41)	20.56(3.28)	20.76(3.45)
	MARD	9.53(1.65)	12.93(3.58)	10.46(1.51)	10.81(1.95)
	MAE	13.89(1.60)	16.28(2.38)	14.49(2.25)	14.86(2.46)
	gRMSE	24.65(3.26)	30.60(6.96)	25.28(4.34)	26.05(4.68)
	Time Lag	5.11(4.38)	6.60(5.13)	10.34(4.07)	9.43(3.99)
ABC4D	RMSE	19.87(2.58)	22.42(4.06)	20.22(3.13)	20.44(3.23)
	MARD	9.79(1.71)	12.51(3.33)	10.44(1.51)	10.85(1.94)
	MAE	14.15(1.64)	15.69(2.10)	14.38(2.21)	14.76(2.37)
	gRMSE	24.83(3.29)	28.71(6.37)	24.72(4.07)	25.55(4.32)
	Time Lag	5.44(4.20)	6.77(4.97)	10.29(3.85)	9.48(3.87)
CTR3	RMSE	20.06(2.57)	22.87(4.20)	20.02(3.06)	20.54(3.28)
	MARD	9.79(1.65)	12.83(3.59)	10.24(1.46)	10.85(1.93)
	MAE	14.24(1.56)	16.01(2.27)	14.17(2.14)	14.83(2.40)
	gRMSE	25.39(3.37)	29.72(6.65)	24.70(4.01)	25.97(4.46)
	Time Lag	4.85(3.92)	6.14(4.71)	9.21(3.66)	8.55(3.65)
REPLACE-BG	RMSE	19.75(2.59)	22.70(4.14)	20.17(3.19)	20.31(3.27)
	MARD	9.47(1.65)	12.45(3.33)	10.22(1.50)	10.50(1.88)
	MAE	13.88(1.62)	15.69(2.12)	14.21(2.22)	14.49(2.35)
	gRMSE	24.56(3.35)	29.15(6.54)	24.55(4.14)	25.24(4.37)
	Time Lag	5.45(4.27)	6.71(4.97)	10.38(3.98)	9.50(3.93)

Bold: results for seen patients (diagonal);
 Un-Bold: results for unseen patients (non-diagonal);
 Red: differences between seen patients and unseen patients are below 0.30 for each column;
 Blue: differences between seen patients and unseen patients are between (0.3, 0.5) for each column.

of 0.50, 0.64, 0.59, and 0.87 mg/dL across the OhioT1DM, ABC4D, CTR3, and REPLACE-BG datasets, respectively, indicating a superior performance relative to “GluADFL(Ring)”, with “GluADFL(Cluster)” maintaining a performance level that is between the two.

We detail the comparative results of prediction performance across diverse methods, as captured in Table 4. This table illustrates the efficacy of each method when trained

on a specified dataset and subsequently tested on both seen (identical dataset) and unseen (alternative datasets) patient data. This comparison aims to evaluate the generalizability of each model comprehensively. The performance of the LSTM model, trained through supervised learning, is highlighted in bold, establishing a benchmark for comparison. Discrepancies from this benchmark are indicated visually in red for differences ≤ 30 and in blue for differences within the (30, 50] range.

- Among the evaluated population models LR, XG-Boost, LSTM, N-BEATS and NHITS, the LSTM model outperforms in terms of accuracy for both seen and unseen patient data. LR and XGBoost are the least effective, while N-BEATS and NHITS lag slightly behind LSTM, with 80% and 75% of their results showing only a 0.3 disparity with LSTM for seen and unseen patients, respectively.
- In the context of meta-learning and FL versus traditional supervised learning, meta-learning methods do not significantly surpass the benchmark. FL-based methodologies, particularly FedAVG and “GluADFL(Random)”, achieve results comparable to supervised learning, with 95% of their outcomes differing from LSTM’s by 0.3 across both seen and unseen patient data scenarios. “GluADFL(Ring)” shows relatively lower effectiveness, with 60% and 65% of its results showing

a 0.3 difference from LSTM for seen and unseen patients, respectively. “GluADFL(Cluster)” is positioned intermediate between “GluADFL(Random)” and “GluADFL(Ring)” in terms of performance.

5. Discussions

5.1. Cross prediction of population models towards unseen patients using federated learning

Recent advancements in deep learning have embraced methodologies such as transfer learning [54, 55, 48] and meta-learning [56, 57] to enhance the prediction of BG levels. These approaches have shown promise by optimizing population models through the application of insights gained across patient groups.

However, a notable drawback of transfer learning and meta-learning lies in their implications for patient privacy, necessitating the collection and aggregation of patient data. Additionally, both transfer learning and meta-learning require data from unseen patients for individual adaptation, conflicting with the preference for adaptation-free population models.

In the literature, population-based LSTM models have been recognized for their ability to accurately model the dynamics of BG levels across diverse patient groups, thereby delivering commendable outcomes in BGLP tasks [12]. These models achieve this by discerning and applying general patterns across datasets without the need for individualized transfer adaptations. This characteristic enables them to effectively predict BG levels in patients not previously seen during training [7]. In our experiments, we also utilized four distinct datasets of varying population sizes, aim to validate the cross-prediction capabilities of population LSTMs for unseen patients, as detailed in Table 3. The results demonstrate that these models, when trained and tested across different datasets, exhibit comparable performance. This consistency in performance extends to experiments involving “GluADFL (Random)”, reinforcing the notion that population LSTMs, when trained through FL, retain their predictive accuracy in BGLP for unseen patients, as shown in Table 2.

Additionally, seen patients whose data are included in the training set can further refine and personalize the population model post FL training, as illustrated in Figure 3. Such customization is achieved by adjusting the model parameters to better fit the individual’s unique data, thereby enhancing the model’s accuracy and effectiveness for their specific BG level predictions. However, the distinction between “Population Model” and “Personalized from Population” is slight, highlighting population features are more important. Therefore, we opt not to focus on personalized FL in current work.

5.2. The impact of different communication topologies of GLuADFL on BGLP

We explore three sparse communication topologies for decentralized FL, specifically ring, cluster, and random, as

suggested in [24, 25]. In Figure 4, with a communication batch size of $B = 7$, we observe some differences in the training efficacy of decentralized FL based on the communication graph topology. The random topology demonstrates the best convergence, i.e., converging at the lowest RMSE, followed by the cluster topology, with the ring topology showing relatively the worst convergence.

This pattern can be attributed to the number of connections in each topology; more connections typically result in better convergence, i.e., converging at lower RMSE. The cluster topology, with its moderate number of connections, converges better than the ring topology but worse than the random topology. The random topology’s time-varying connections facilitate wider broadcasting of model parameters, leading to its best convergence.

Moreover, as the population size increases (from OhioT1DM to REPLACE-BG), the differences in convergence performance among these topologies become more notable. Specifically, topologies with fewer connections, like the ring topology, tend to transmit model parameters more slowly and limited during communications.

Additionally, we implement a wait-free mechanism, as discussed in [25], where only active nodes participate in communication and local model updates. Figure 5 reveals the impact of inactive node ratios on the prediction performance across different communication topologies. In line with our earlier observations, the random topology maintains stability even as the inactive node ratio increases. Notably, larger datasets amplify the advantages of the random topology, showing more significant performance gaps compared to other topologies. Figure 5 also indicates a sharp decline in the effectiveness of GluADFL when the inactive node ratio exceeds 70%.

These observations reveal that our GluADFL framework adapts well to varying network topologies, with the random topology showing particular resilience in unstable or dynamic network conditions. Its robust performance, even with a high inactive node ratio, demonstrates its potential for real-world applications where network scenarios are variable for different social preferences. The observed scalability with larger datasets reinforces GluADFL’s suitability for extensive decentralized learning environments.

5.3. Comparison of blood glucose prediction performance

In comparing GluADFL with baselines on four datasets for both seen and unseen patients (see Section 4.4, Tables 4), we observed the following:

1) LSTM models outperform traditional algorithms like LR and XGBoost in BGLP. Despite the effectiveness of LR and XGBoost in BGLP as documented in [58, 59], they fall short in comparison to LSTM in all metrics for both seen and unseen patients. Advanced deep learning models like N-BEATS and NHiTS, though excellent in healthcare applications [60, 61], do not surpass LSTM when using only BG data as input, similar to findings in [62]. This could be

Table 4
Blood Glucose Prediction for Seen/Unseen Patients by Different Population Methods on Four Datasets

Training Data	Metrics	Methods Tested by Seen Patients										
		LR	XGBoost	LSTM	N-BEATS	NHITS	MAML	MetaSGD	FedAvg	GluADFL(Ring)	GluADFL(Cluster)	GluADFL(Random)
OhioT1DM	RMSE	21.48(5.38)	20.64(3.72)	19.65(3.59)	19.94(3.82)	19.89(3.75)	20.68(3.81)	20.44(3.87)	19.65(3.60)	19.74(3.63)	19.65(3.58)	19.66(3.59)
	MARD	10.52(2.67)	10.18(2.32)	9.53(2.19)	9.64(2.31)	9.66(2.28)	9.97(2.21)	10.23(2.42)	9.43(2.22)	9.52(2.24)	9.47(2.24)	9.43(2.23)
	MAE	15.28(3.08)	14.76(2.60)	13.89(2.45)	14.08(2.58)	14.06(2.54)	14.77(2.61)	14.74(2.65)	13.78(2.44)	13.87(2.46)	13.81(2.44)	13.80(2.44)
	gRMSE	26.94(7.44)	26.07(5.16)	24.65(5.02)	25.00(5.34)	24.83(5.23)	25.81(5.37)	25.10(5.32)	24.45(5.02)	24.57(5.07)	24.46(4.99)	24.61(5.03)
	Time Lag	7.17(4.90)	6.63(4.86)	5.11(4.29)	5.67(4.37)	5.76(4.42)	5.88(4.39)	5.75(4.33)	5.34(4.29)	5.40(4.29)	5.41(4.30)	5.22(4.28)
ABC4D	RMSE	27.14(4.40)	23.56(3.60)	22.42(3.33)	22.92(3.45)	22.67(3.41)	22.99(3.43)	23.23(3.49)	22.27(3.33)	22.73(3.43)	22.42(3.36)	22.28(3.33)
	MARD	14.70(2.60)	13.16(2.31)	12.51(2.12)	12.64(2.17)	12.30(2.08)	12.75(2.15)	12.54(2.06)	12.26(2.07)	12.57(2.14)	12.43(2.12)	12.16(2.04)
	MAE	18.68(3.06)	16.45(2.56)	15.69(2.33)	15.85(2.39)	15.64(2.34)	16.23(2.45)	16.34(2.51)	15.44(2.30)	15.77(2.37)	15.57(2.33)	15.41(2.30)
	gRMSE	35.54(6.15)	30.75(5.01)	28.71(4.58)	29.74(4.82)	29.08(4.70)	29.50(4.74)	30.06(4.92)	28.57(4.58)	29.03(4.69)	28.77(4.62)	28.60(4.59)
	Time Lag	9.59(5.61)	7.93(4.75)	6.77(4.14)	6.76(4.25)	6.85(4.25)	6.60(4.20)	6.29(4.21)	6.74(4.20)	7.32(4.42)	6.87(4.27)	6.69(4.16)
CTR3	RMSE	22.95(4.67)	20.83(3.59)	20.02(3.39)	20.09(3.49)	20.13(3.44)	20.54(3.52)	20.55(3.54)	20.00(3.40)	20.30(3.49)	20.07(3.42)	20.00(3.40)
	MARD	11.67(2.58)	10.70(2.35)	10.24(2.17)	10.25(2.26)	10.29(2.21)	10.71(2.37)	10.79(2.43)	10.08(2.12)	10.28(2.17)	10.16(2.17)	10.09(2.12)
	MAE	16.08(2.96)	14.77(2.52)	14.17(2.37)	14.17(2.39)	14.22(2.37)	14.65(2.46)	14.69(2.47)	14.04(2.33)	14.27(2.37)	14.11(2.35)	14.03(2.32)
	gRMSE	28.53(6.54)	25.81(5.01)	24.70(4.75)	24.72(4.90)	24.60(4.79)	25.00(4.89)	24.90(4.89)	24.47(4.75)	24.70(4.85)	24.50(4.79)	24.42(4.74)
	Time Lag	13.13(4.99)	11.69(4.59)	9.21(3.89)	9.43(3.97)	9.60(4.02)	10.19(4.18)	9.96(4.11)	9.72(4.02)	10.48(4.23)	9.86(4.07)	9.76(4.04)
REPLACE-BG	RMSE	23.31(4.73)	21.21(3.59)	20.31(3.39)	20.43(3.51)	20.42(3.48)	21.82(3.68)	21.44(3.61)	20.33(3.45)	20.87(3.64)	20.70(3.58)	20.34(3.46)
	MARD	11.85(2.54)	11.18(2.27)	10.50(2.09)	10.50(2.16)	10.43(2.09)	12.58(2.77)	11.27(2.26)	10.43(2.11)	10.75(2.23)	10.69(2.21)	10.45(2.12)
	MAE	16.34(2.95)	15.24(2.51)	14.49(2.32)	14.50(2.37)	14.49(2.36)	16.32(2.73)	15.60(2.58)	14.42(2.34)	14.80(2.46)	14.70(2.43)	14.44(2.34)
	gRMSE	29.39(6.61)	26.75(4.96)	25.24(4.68)	25.46(4.88)	25.44(4.82)	27.99(5.21)	27.40(5.17)	25.36(4.80)	25.98(5.05)	25.85(4.98)	25.38(4.81)
	Time Lag	12.19(5.02)	11.08(4.69)	9.50(4.21)	9.63(4.24)	9.87(4.28)	8.40(4.05)	8.88(4.12)	9.45(4.22)	10.49(4.48)	10.14(4.42)	9.46(4.22)
Training Data	Metrics	Methods Tested by ALL Other Unseen Patients										
		LR	XGBoost	LSTM	N-BEATS	NHITS	MAML	MetaSGD	FedAvg	GluADFL(Ring)	GluADFL(Cluster)	GluADFL(Random)
OhioT1DM	RMSE	24.50(5.38)	21.72(3.72)	20.99(3.59)	21.52(3.82)	21.41(3.75)	22.23(3.81)	22.17(3.87)	20.97(3.60)	21.08(3.63)	20.94(3.58)	20.96(3.59)
	MARD	12.16(2.67)	11.51(2.32)	10.96(2.19)	11.15(2.31)	11.14(2.28)	11.38(2.21)	11.84(2.42)	10.89(2.22)	10.95(2.24)	10.91(2.24)	10.88(2.23)
	MAE	16.60(3.08)	15.57(2.60)	14.94(2.45)	15.23(2.58)	15.17(2.54)	15.86(2.61)	15.98(2.65)	14.85(2.44)	14.92(2.46)	14.85(2.44)	14.85(2.44)
	gRMSE	30.99(7.44)	27.52(5.16)	26.37(5.02)	27.04(5.34)	26.82(5.23)	27.75(5.37)	27.36(5.32)	26.19(5.02)	26.35(5.07)	26.15(4.99)	26.30(5.03)
	Time Lag	11.60(4.90)	11.25(4.86)	9.28(4.29)	9.67(4.37)	9.93(4.42)	9.72(4.39)	9.62(4.33)	9.36(4.29)	9.33(4.29)	9.37(4.30)	9.25(4.28)
ABC4D	RMSE	23.69(4.40)	21.35(3.60)	20.39(3.33)	20.51(3.45)	20.43(3.41)	20.95(3.43)	21.24(3.49)	20.17(3.33)	20.46(3.43)	20.26(3.36)	20.18(3.33)
	MARD	12.53(2.60)	11.38(2.31)	10.75(2.12)	10.67(2.17)	10.51(2.08)	11.09(2.15)	10.99(2.06)	10.43(2.07)	10.63(2.14)	10.52(2.12)	10.36(2.04)
	MAE	17.21(3.06)	15.46(2.56)	14.69(2.33)	14.66(2.39)	14.56(2.34)	15.28(2.45)	15.45(2.51)	14.40(2.30)	14.64(2.37)	14.48(2.33)	14.37(2.30)
	gRMSE	30.12(6.15)	27.14(5.00)	25.43(4.58)	25.77(4.82)	25.39(4.70)	26.19(4.74)	26.85(4.92)	25.11(4.58)	25.31(4.69)	25.21(4.62)	25.18(4.59)
	Time Lag	14.01(5.61)	11.15(4.75)	9.39(4.14)	9.62(4.25)	9.70(4.25)	9.18(4.20)	9.10(4.21)	9.47(4.20)	10.28(4.42)	9.69(4.27)	9.42(4.16)
CTR3	RMSE	23.72(4.67)	21.39(3.59)	20.74(3.39)	20.78(3.49)	20.71(3.44)	21.16(3.52)	21.20(3.54)	20.52(3.40)	20.73(3.49)	20.61(3.42)	20.49(3.40)
	MARD	12.23(2.58)	11.47(2.35)	10.99(2.17)	10.97(2.26)	10.94(2.21)	11.51(2.37)	11.65(2.43)	10.65(2.12)	10.79(2.17)	10.79(2.17)	10.64(2.12)
	MAE	16.67(2.96)	15.40(2.52)	14.91(2.37)	14.84(2.39)	14.81(2.37)	15.29(2.46)	15.37(2.47)	14.56(2.33)	14.71(2.37)	14.67(2.35)	14.54(2.32)
	gRMSE	30.17(6.54)	27.26(5.01)	26.30(4.75)	26.27(4.90)	26.00(4.79)	26.47(4.89)	26.41(4.89)	25.80(4.75)	25.92(4.85)	25.92(4.79)	25.72(4.74)
	Time Lag	11.48(4.99)	10.10(4.59)	8.15(3.89)	8.23(3.97)	8.41(4.02)	8.90(4.18)	8.69(4.11)	8.53(4.02)	9.13(4.23)	8.64(4.07)	8.59(4.04)
REPLACE-BG	RMSE	24.69(4.73)	21.93(3.59)	21.04(3.39)	21.24(3.51)	21.20(3.48)	22.17(3.68)	21.97(3.61)	21.13(3.45)	21.78(3.64)	21.56(3.58)	21.14(3.46)
	MARD	12.45(2.54)	11.52(2.27)	10.92(2.09)	10.96(2.16)	10.85(2.09)	12.70(2.77)	11.58(2.26)	10.89(2.11)	11.27(2.23)	11.18(2.21)	10.91(2.12)
	MAE	16.75(2.95)	15.40(2.51)	14.70(2.32)	14.75(2.37)	14.72(2.36)	16.17(2.73)	15.61(2.58)	14.68(2.34)	15.14(2.46)	15.00(2.43)	14.69(2.34)
	gRMSE	31.27(6.61)	27.69(4.96)	26.27(4.68)	26.62(4.88)	26.53(4.82)	28.39(5.21)	28.09(5.17)	26.48(4.80)	27.23(5.05)	27.03(4.98)	26.50(4.81)
	Time Lag	10.52(5.02)	9.56(4.69)	8.13(4.21)	8.18(4.24)	8.44(4.28)	7.18(4.05)	7.60(4.12)	8.09(4.22)	9.00(4.48)	8.68(4.42)	8.12(4.22)

Bold: results for LSTM trained by supervised learning;
Red: differences between LSTM trained by supervised learning and other methods are below 0.30 for each row;
Blue: differences between LSTM trained by supervised learning and other methods are between (0.3, 0.5] for each row.

because N-BEATS and NHITS are more suited for complex time series forecasting than single point predictions.

2) Population FL-based LSTMs have inherent generalization and cross-predictive capabilities for unseen patients, as seen in section 5.1. We test meta-learning approaches like MAML and MetaSGD, known for quick adaptation to new tasks, in our baseline models without fine-tuning for unseen patients. However, these meta-learning models cannot outperform LSTM, FedAvg, or GluADFL for unseen patients. Consequently, we decide against incorporating a meta-learning module in GluADFL and did not pursue meta-learning-based FL [63] or domain generation-based FL [64] further.

3) GluADFL shows comparable performance to FedAvg, indicating that the FL and decentralized structure do not compromise LSTM’s modeling and cross-predictive abilities. GluADFL also addresses the “cold start” problem in BGLP, enabling cross-prediction for unseen patients while protecting privacy. Therefore, we choose not to add complex modules to GluADFL, such as masked model-parameter averaging [24] or client-communication weight selection [25].

6. Limitations and Future work

This study, while contributing valuable insights into BGLP using FL and population LSTM models, acknowledges certain limitations that present areas for future exploration.

Our current investigation is confined to single-horizon BG level predictions, and does not extend to multi-horizon forecasting. Multi-horizon prediction involves estimating BG levels at multiple future time points, offering a more comprehensive view of glucose fluctuations over time. This limitation highlights a significant area for further research, where expanding the scope to include multi-horizon predictions could enhance the utility of our models for more dynamic and anticipatory diabetes management.

The exploration of our proposed method is focused primarily on BGLP and has yet to encompass other critical areas of diabetes management, such as insulin dose recommendation, dietary advice, or physical activity impact analysis. The complexity and multifaceted nature of diabetes care suggest a wealth of opportunities for applying our methodology to other aspects of diabetes management, potentially offering a more holistic approach to managing the condition.

The focus of this work is on designing an FL training framework. Therefore, we adopted LSTM as a basic deep learning-based approach in BGLP and will more advanced

models like those based on transformers [16, 40, 65, 66, 67], in the future.

7. Conclusions

To address the “cold start” problem in BGLP while ensuring privacy, we propose GluADFL, an asynchronous decentralized FL framework. We employed LSTMs as a practical and efficient solution for individual patient BG level predictions. Using four T1D datasets, we demonstrated GluADFL’s ability to maintain LSTM’s cross-predictive capacity, showing scalability with larger populations and robustness across various communication topologies and asynchronous settings. Hence, we successfully established a robust and privacy-preserving approach to BGLP, offering both high accuracy and adherence to privacy considerations.

8. Acknowledgement

We thank the support from UKRI Center for Doctoral Training in AI-enabled healthcare systems [EP/S021612/1] and University College London Overseas Research Scholarships. We also appreciate the support from Rosetrees Trust (Grant number: UCL-IHE-2020\102) and Great Ormond Street Hospital (Charity ref.X12018). The study sponsors had no study involvement.

References

- [1] I. Contreras, A. Bertachi, L. Biagi, J. Vehí, S. Oviedo, Using grammatical evolution to generate short-term blood glucose prediction models, in: *IJCAI-ECAI’18*, volume 2148, 2018, pp. 91–96.
- [2] E. Montaser, J. Díez, J. Bondia, Glucose prediction under variable-length time-stamped daily events: A seasonal stochastic local modeling framework, *Sensors* 21 (2021) 3188. doi:10.3390/S21093188.
- [3] T. Zhu, L. Kuang, J. Daniels, P. Herrero, K. Li, P. Georgiou, Iomt-enabled real-time blood glucose prediction with deep learning and edge computing, *IEEE Internet Things J.* 10 (2023) 3706–3719. doi:10.1109/JIOT.2022.3143375.
- [4] P. G. Jacobs, P. Herrero, A. Facchinetti, J. Vehí, B. Kovatchev, M. D. Breton, A. Cinar, K. S. Nikita, F. J. Doyle, J. Bondia, T. Battelino, J. R. Castle, K. Zarkogianni, R. Narayan, C. Mosquera-Lopez, Artificial intelligence and machine learning for improving glycemic control in diabetes: Best practices, pitfalls, and opportunities, *IEEE Reviews in Biomedical Engineering* 17 (2024) 19–41. doi:10.1109/RBME.2023.3331297.
- [5] E. Pellizzari, F. Prendin, G. Cappon, G. Sparacino, A. Facchinetti, A deep-learning based algorithm for the management of hyperglycemia in type 1 diabetes therapy, in: *IEEE BSN’23*, 2023, pp. 1–4. doi:10.1109/BSN58485.2023.10330994.
- [6] M. Desgrouas, J. Demiselle, L. Stiel, V. Brunot, R. Marnai, S. Sarfati, M. Fiancette, F. Lambiotte, A. W. Thille, M. Leloup, et al., Insulin therapy and blood glucose management in critically ill patients: a 1-day cross-sectional observational study in 69 french intensive care units, *Annals of Intensive Care* 13 (2023) 1–13.
- [7] A. Mohebbi, A. R. Johansen, N. Hansen, P. E. Christensen, J. M. Tarp, M. L. Jensen, H. Bengtsson, M. Mørup, Short term blood glucose prediction based on continuous glucose monitoring data, in: *IEEE EMBC’20*, 2020, pp. 5140–5145. doi:10.1109/EMBC44109.2020.9176695.
- [8] A. Lakhan, M. A. Mohammed, J. Nedoma, R. Martinek, P. Tiwari, A. Vidyarthi, A. Alkhayat, W. Wang, Federated-learning based privacy preservation and fraud-enabled blockchain iomt system for healthcare, *IEEE J. Biomed. Health Informatics* 27 (2023) 664–672. doi:10.1109/JBHI.2022.3165945.
- [9] B. McMahan, E. Moore, D. Ramage, S. Hampson, B. A. y Arcas, Communication-efficient learning of deep networks from decentralized data, in: *AISTATS’17*, volume 54, 2017, pp. 1273–1282.
- [10] Y. Xian, C. H. Lampert, B. Schiele, Z. Akata, Zero-shot learning - A comprehensive evaluation of the good, the bad and the ugly, *IEEE Trans. Pattern Anal. Mach. Intell.* 41 (2019) 2251–2265. doi:10.1109/TPAMI.2018.2857768.
- [11] C. Marling, R. C. Bunesco, The ohio1dm dataset for blood glucose level prediction: Update 2020, in: *KDH@ECAI’20*, volume 2675, 2020, pp. 71–74.
- [12] R. Bevan, F. Coenen, Experiments in non-personalized future blood glucose level prediction, in: *KDH@ECAI’20*, volume 2675, 2020, pp. 100–104.
- [13] T. Yang, R. Wu, R. Tao, S. Wen, N. Ma, Y. Zhao, X. Yu, H. Li, Multi-scale long short-term memory network with multi-lag structure for blood glucose prediction, in: *KDH@ECAI’20*, volume 2675, 2020, pp. 136–140.
- [14] B. N. Oreshkin, D. Carпов, N. Chapados, Y. Bengio, N-BEATS: neural basis expansion analysis for interpretable time series forecasting, in: *ICLR’20*, 2020.
- [15] C. Challu, K. G. Olivares, B. N. Oreshkin, F. G. Ramírez, M. M. Canseco, A. Dubrawski, NHITS: neural hierarchical interpolation for time series forecasting, in: *AAAI’23*, 2023, pp. 6989–6997. doi:10.1609/AAAI.V37I6.25854.
- [16] A. Vaswani, N. Shazeer, N. Parmar, J. Uszkoreit, L. Jones, A. N. Gomez, L. Kaiser, I. Polosukhin, Attention is all you need, in: *NeurIPS’17*, 2017, pp. 5998–6008.
- [17] T. Chen, C. Guestrin, Xgboost: A scalable tree boosting system, in: *KDD’16*, 2016, pp. 785–794. doi:10.1145/2939672.2939785.
- [18] C. Finn, P. Abbeel, S. Levine, Model-agnostic meta-learning for fast adaptation of deep networks, in: *ICML’17*, volume 70, 2017, pp. 1126–1135.
- [19] Z. Li, F. Zhou, F. Chen, H. Li, Meta-sgd: Learning to learn quickly for few shot learning, *CoRR abs/1707.09835* (2017).
- [20] C. He, E. Ceyani, K. Balasubramanian, M. Annavam, S. Avestimehr, Spreadgnn: Decentralized multi-task federated learning for graph neural networks on molecular data, in: *AAAI’22*, 2022, pp. 6865–6873. doi:10.1609/AAAI.V36I6.20643.
- [21] Y. Shi, L. Shen, K. Wei, Y. Sun, B. Yuan, X. Wang, D. Tao, Improving the model consistency of decentralized federated learning, in: *ICML’23*, volume 202, 2023, pp. 31269–31291.
- [22] W. Liu, L. Chen, W. Wang, General decentralized federated learning for communication-computation tradeoff, in: *IEEE INFOCOM’22*, 2022, pp. 1–6. doi:10.1109/INFOCOMWKSHPS54753.2022.9797891.
- [23] M. Chen, Y. Xu, H. Xu, L. Huang, Enhancing decentralized federated learning for non-iid data on heterogeneous devices, in: *IEEE ICDE’23*, 2023, pp. 2289–2302. doi:10.1109/ICDE55515.2023.00177.
- [24] R. Dai, L. Shen, F. He, X. Tian, D. Tao, Displf: Towards communication-efficient personalized federated learning via decentralized sparse training, in: *ICML’22*, volume 162, 2022, pp. 4587–4604.
- [25] M. Bornstein, T. Rabbani, E. Wang, A. S. Bedi, F. Huang, SWIFT: rapid decentralized federated learning via wait-free model communication, in: *ICLR’23*, 2023.
- [26] D. H. Hagos, E. Tankard, D. B. Rawat, A scalable asynchronous federated learning for privacy-preserving real-time surveillance systems, in: *IEEE INFOCOM’23*, 2023, pp. 1–6. doi:10.1109/INFOCOMWKSHPS57453.2023.10226108.
- [27] S. Jang, H. Lim, Asyncnfl: Asynchronous federated learning using majority voting with quantized model updates (student abstract), in: *AAAI’22*, 2022, pp. 12975–12976. doi:10.1609/AAAI.V36I11.21624.
- [28] H. Yang, X. Zhang, P. Khanduri, J. Liu, Anarchic federated learning, in: *ICML’22*, volume 162, 2022, pp. 25331–25363.
- [29] N. B. Truong, K. Sun, S. Wang, F. Guitton, Y. Guo, Privacy preservation in federated learning: An insightful survey from the GDPR perspective, *Comput. Secur.* 110 (2021) 102402. doi:10.1016/

J.COSE.2021.102402.

- [30] M. Joshi, A. Pal, M. Sankarasubbu, Federated learning for healthcare domain - pipeline, applications and challenges, *ACM Trans. Comput. Healthcare* 3 (2022). doi:10.1145/3533708.
- [31] M. Akter, N. Moustafa, T. M. Lynar, I. Razzak, Edge intelligence: Federated learning-based privacy protection framework for smart healthcare systems, *IEEE J. Biomed. Health Informatics* 26 (2022) 5805–5816. doi:10.1109/JBHI.2022.3192648.
- [32] A. Rahman, M. S. Hossain, G. Muhammad, D. Kundu, T. Debnath, M. S. Rahman, M. S. I. Khan, P. Tiwari, S. S. Band, Federated learning-based AI approaches in smart healthcare: concepts, taxonomies, challenges and open issues, *Clust. Comput.* 26 (2023) 2271–2311. doi:10.1007/S10586-022-03658-4.
- [33] P. He, C. Lan, A. K. Bashir, D. Wu, R. Wang, R. Kharel, K. Yu, Low-latency federated learning via dynamic model partitioning for healthcare iot, *IEEE J. Biomed. Health Informatics* 27 (2023) 4684–4695. doi:10.1109/JBHI.2023.3298446.
- [34] B. Dolo, F. Loukil, K. Boukadi, Early detection of diabetes mellitus using differentially private SGD in federated learning, in: *IEEE AICCSA'22*, 2022, pp. 1–8. doi:10.1109/AICCSA56895.2022.10017908.
- [35] Y. Su, C. Huang, W. Zhu, X. Lyu, F. Ji, Multi-party diabetes mellitus risk prediction based on secure federated learning, *Biomed. Signal Process. Control.* 85 (2023) 104881. doi:10.1016/J.BSPC.2023.104881.
- [36] X. Guo, Q. Yao, J. T. Kwok, W. Tu, Y. Chen, W. Dai, Q. Yang, Privacy-preserving stacking with application to cross-organizational diabetes prediction, in: *Federated Learning - Privacy and Incentive*, volume 12500, 2020, pp. 269–283. doi:10.1007/978-3-030-63076-8_19.
- [37] I. D. Falco, A. D. Cioppa, T. Koutny, M. Ubl, M. Krma, U. Scafuri, E. Tarantino, A federated learning-inspired evolutionary algorithm: Application to glucose prediction, *Sensors* 23 (2023) 2957. doi:10.3390/S23062957.
- [38] S. Canali, V. Schiaffonati, A. Aliverti, Challenges and recommendations for wearable devices in digital health: Data quality, interoperability, health equity, fairness, *PLOS Digital Health* 1 (2022) e0000104. doi:10.1371/journal.pdig.0000104.
- [39] V. Sameera, A. Bindra, G. P. Rath, Human errors and their prevention in healthcare, *Journal of Anaesthesiology, Clinical Pharmacology* 37 (2021) 328. doi:10.4103/joacp.JOACP_364_19.
- [40] T. Zhu, T. Chen, L. Kuang, J. Zeng, K. Li, P. Georgiou, Edge-based temporal fusion transformer for multi-horizon blood glucose prediction, in: *IEEE ISCAS'23*, 2023, pp. 1–5. doi:10.1109/ISCAS46773.2023.10181448.
- [41] C. Piao, K. Li, Blood glucose level prediction: A graph-based explainable method with federated learning, *arXiv preprint arXiv:2312.12541* (2023).
- [42] F. Prendin, J. Pavan, G. Cappon, S. Del Favero, G. Sparacino, A. Facchinetti, The importance of interpreting machine learning models for blood glucose prediction in diabetes: an analysis using shap, *Scientific Reports* 13 (2023) 16865.
- [43] A. D. Zahedani, A. Veluvali, T. McLaughlin, N. Aghaeepour, A. Hoseinian, S. Agarwal, J. Ruan, S. Tripathi, M. Woodward, N. Hashemi, M. Snyder, Digital health application integrating wearable data and behavioral patterns improves metabolic health, *npj Digit. Medicine* 6 (2023). doi:10.1038/s41746-023-00956-Y.
- [44] S. Hochreiter, J. Schmidhuber, Long short-term memory, *Neural Comput.* 9 (1997) 1735–1780. doi:10.1162/NECO.1997.9.8.1735.
- [45] M. Reddy, P. Pesl, M. Xenou, C. Toumazou, D. Johnston, P. Georgiou, P. Herrero, N. Oliver, Clinical safety and feasibility of the advanced bolus calculator for type 1 diabetes based on case-based reasoning: A 6-week nonrandomized single-arm pilot study, *Diabetes Technology & Therapeutics* 18 (2016) 487–493. doi:10.1089/dia.2015.0413.
- [46] G. Aleppo, K. J. Ruedy, T. D. Riddlesworth, D. F. Kruger, A. L. Peters, I. Hirsch, R. M. Bergenstal, E. Toschi, A. J. Ahmann, V. N. Shah, M. R. Rickels, B. W. Bode, A. Philis-Tsimikas, R. Pop-Busui, H. Rodriguez, E. Eyth, A. Bhargava, C. Kollman, R. W. Beck, R.-B. S. Group, Replace-bg: A randomized trial comparing continuous glucose monitoring with and without routine blood glucose monitoring in adults with well-controlled type 1 diabetes, *Diabetes Care* 40 (2017) 538–545. doi:10.2337/dc16-2482.
- [47] S. D. Favero, A. Facchinetti, C. Cobelli, A glucose-specific metric to assess predictors and identify models, *IEEE Trans. Biomed. Eng.* 59 (2012) 1281–1290. doi:10.1109/TBME.2012.2185234.
- [48] T. Zhu, C. Uduku, K. Li, P. Herrero, N. Oliver, P. Georgiou, Enhancing self-management in type 1 diabetes with wearables and deep learning, *npj Digital Medicine* 5 (2022) 78. doi:10.1038/s41746-022-00626-5.
- [49] L. Cohen, *Time-frequency analysis*, volume 778, Prentice hall New Jersey, 1995.
- [50] A. Gani, A. V. Gribok, Y. Lu, W. K. Ward, R. A. Vigersky, J. Reifman, Universal glucose models for predicting subcutaneous glucose concentration in humans, *IEEE Trans. Inf. Technol. Biomed.* 14 (2010) 157–165. doi:10.1109/TITB.2009.2034141.
- [51] K. Li, C. Liu, T. Zhu, P. Herrero, P. Georgiou, Glunet: A deep learning framework for accurate glucose forecasting, *IEEE J. Biomed. Health Informatics* 24 (2020) 414–423. doi:10.1109/JBHI.2019.2931842.
- [52] S. M. Arnold, P. Mahajan, D. Datta, I. Bunner, learn2learn, 2019. URL: <https://github.com/learnables/learn2learn>.
- [53] L. Buitinck, G. Louppe, M. Blondel, F. Pedregosa, A. Mueller, O. Grisel, V. Niculae, P. Prettenhofer, A. Gramfort, J. Grobler, R. Layton, J. VanderPlas, A. Joly, B. Holt, G. Varoquaux, API design for machine learning software: experiences from the scikit-learn project, in: *ECML PKDD Workshop: Languages for Data Mining and Machine Learning*, 2013, pp. 108–122.
- [54] T. Zhu, K. Li, J. Chen, P. Herrero, P. Georgiou, Dilated recurrent neural networks for glucose forecasting in type 1 diabetes, *J. Heal. Informatics Res.* 4 (2020) 308–324. doi:10.1007/S41666-020-00068-2.
- [55] X. Yu, T. Yang, J. Lu, Y. Shen, W. Lu, W. Zhu, Y. Bao, H. Li, J. Zhou, Deep transfer learning: a novel glucose prediction framework for new subjects with type 2 diabetes, *Complex & Intelligent Systems* 8 (2021) 1–13. doi:10.1007/s40747-021-00360-7.
- [56] T. Zhu, K. Li, P. Herrero, P. Georgiou, Personalized blood glucose prediction for type 1 diabetes using evidential deep learning and meta-learning, *IEEE Transactions on Biomedical Engineering* 70 (2023) 193–204. doi:10.1109/TBME.2022.3187703.
- [57] S. Langarica, M. Rodriguez-Fernandez, F. Nunez, F. J. Doyle III, A meta-learning approach to personalized blood glucose prediction in type 1 diabetes, *Control Engineering Practice* 135 (2023) 105498.
- [58] Z. Zhang, A mathematical model for predicting glucose levels in critically-ill patients: The pignoli model, *PeerJ* 3 (2015) e1005. doi:10.7717/peerj.1005.
- [59] G. Alfian, M. Syafrudin, J. Rhee, M. Anshari, M. Mustakim, I. Fahrurrozi, Blood glucose prediction model for type 1 diabetes based on extreme gradient boosting, *IOP Conference Series: Materials Science and Engineering* 803 (2020) 012012. doi:10.1088/1757-899X/803/1/012012.
- [60] H. Rubin-Falcone, I. Fox, J. Wiens, Deep residual time-series forecasting: Application to blood glucose prediction, in: *KDH@ECAI'20*, volume 2675, 2020, pp. 105–109.
- [61] W. Potosnak, C. Challu, K. G. Olivares, A. Dubrawski, Forecasting response to treatment with global deep learning and patient-specific pharmacokinetic priors., *Arxiv* (2023) arXiv-2309.
- [62] B. Puzskarski, K. Hryniów, G. Sarwas, Comparison of neural basis expansion analysis for interpretable time series (n-beats) and recurrent neural networks for heart dysfunction classification, *Physiological Measurement* 43 (2022) 064006.
- [63] F. Chen, M. Luo, Z. Dong, Z. Li, X. He, Federated meta-learning with fast convergence and efficient communication, *arXiv preprint arXiv:1802.07876* (2018).
- [64] R. Zhang, Q. Xu, J. Yao, Y. Zhang, Q. Tian, Y. Wang, Federated domain generalization with generalization adjustment, in: *IEEE/CVF CVPR'23*, 2023, pp. 3954–3963. doi:10.1109/CVPR52729.2023.00385.
- [65] T. Zhu, L. Kuang, C. Piao, J. Zeng, K. Li, P. Georgiou, Population-specific glucose prediction in diabetes care with transformer-based deep learning on the edge, *IEEE Transactions on Biomedical Circuits*

and Systems (2023) 1–12. doi:10.1109/TBCAS.2023.3348844.

- [66] R. Sergazinov, M. Armandpour, I. Gaynanova, Gluformer: Transformer-based personalized glucose forecasting with uncertainty quantification, in: IEEE ICASSP'23, 2023, pp. 1–5. doi:10.1109/ICASSP49357.2023.10096419.
- [67] E. Acuña, R. Aparicio, V. Palomino, Analyzing the performance of transformers for the prediction of the blood glucose level considering imputation and smoothing, Big Data Cogn. Comput. 7 (2023) 41. doi:10.3390/BDCC7010041.